J. Fluid Mech. (1997), *vol.* 351, *pp.* 139–165. Printed in the United Kingdom

Instability of two-layer creeping flow in a channel with parallel-sided walls

By C. POZRIKIDIS

Department of Applied Mechanics and Engineering Sciences, University of California, San Diego, La Jolla, CA 92093-0411, USA
e-mail: costas@ames.ucsd.edu

(Received 12 March 1997 and in revised form 25 June 1997)

The evolution of the interface between two viscous fluid layers in a two-dimensional horizontal channel confined between two parallel walls is considered in the limit of Stokes flow. The motion is generated either by the translation of the walls, in a shear-driven or plane-Couette mode, or by an axial pressure gradient, in a plane-Poiseuille mode. Linear stability analysis for infinitesimal perturbations and fluids with matched densities shows that when the viscosities of the fluids are different and the Reynolds number is sufficiently high, the flow is unstable. At vanishing Reynolds number, the flow is stable when the surface tension has a non-zero value, and neutrally stable when the surface tension vanishes. We investigate the behaviour of the interface subject to finite-amplitude two-dimensional perturbations by solving the equations of Stokes flow using a boundary-integral method. Integral equations for the interfacial velocity are formulated for the three modular cases of shear-driven, pressure-driven, and gravity-driven flow, and numerical computations are performed for the first two modes. The results show that disturbances of sufficiently large amplitude may cause permanent interfacial deformation in which the interface folds, develops elongated fingers, or supports slowly evolving travelling waves. Smaller amplitude disturbances decay, sometimes after a transient period of interfacial folding. The ratio of the viscosities of the two fluids plays an important role in determining the morphology of the emerging interfacial patterns, but the parabolicity of the unperturbed velocity profile does not affect the character of the motion. Increasing the contrast in the viscosities of the two fluids, while keeping the channel capillary number fixed, destabilizes the interfaces; re-examining the flow in terms of an alternative capillary number that is defined with respect to the velocity drop across the more-viscous layer shows that this is a reasonable behaviour. Comparing the numerical results with the predictions of a lubrication-flow model shows that, in the absence of inertia, the simplified approach can only describe a limited range of motions, and that the physical relevance of the steadily travelling waves predicted by long-wave theories must be accepted with a certain degree of reservation.

1. Introduction

Interfaces between two adjacent fluids are susceptible to various kinds of hydrodynamic instabilities with different origins and diverse mechanisms of growth. The Kelvin–Helmholtz instability may be regarded as the instability of a vortex layer established along an interface at high Reynolds numbers; the capillary instability is due to pressure variations generated by the deformation of a corrugated three-dimensional interface; and the Marangoni instability is due to variations in surface tension

produced, for example, by a temperature field or by an uneven distribution of surfactants.

Perhaps the most subtle and poorly understood type of interfacial instability is the one caused by differences in the viscosities of two adjacent fluids in parallel shearing motion. At high Reynolds numbers, the growth of perturbations may be associated with the discontinuity in the vorticity or slope of the unperturbed velocity across the interface, which is necessary in order for the shear stress to remain continuous across the interface. Accordingly, one may argue that viscosity is important only in so far as to establish this discontinuity, and plays a secondary role in the subsequent motion. The growth or decay of interfacial perturbations may then be studied in the context of the equations of inviscid flow under the formalism of vorticity dynamics. Relevant studies include those of the instability of semi-infinite vortex regions, vortex layers of finite thickness, compound vortex layers, and vortex layers attached to walls.

At low and moderate Reynolds numbers, the nominal cause of the instability, and the physical mechanisms by which it proceeds is not as clear. The linear stability analysis of the plane Poiseuille flow of two superposed layers conducted by Yiantsios & Higgins (1988) indicates that, even when viscous forces are significant or dominant, the instability may be still attributed to the discontinuity in the slope of the unperturbed velocity across the interface: when the slope is continuous, the flow is either neutrally stable or stable at any Reynolds number. One may argue that ripples of a viscous fluid adjacent to a less-viscous fluid are sustained for an extended period of time and thus have a better chance to grow.

Hinch (1984) proposed a simple physical explanation for the growth of interfacial waves with short wavelength and infinitesimal amplitude on the flat interface of two parallel streams in shearing motion, in the absence of surface tension. His arguments consider the generation and redistribution of vorticity around the interface, the latter due to convection. It would appear that convective transport is necessary for the onset of an instability due to viscosity striation, and that a slightly perturbed interface will either be neutrally stable or return to its unperturbed position under conditions of Stokes flow, but this is not generally true.

Consider, for example, the motion of a liquid layer down an inclined plane, with another layer of a lubricating fluid of the same density separating it from the plane. When the viscosity of the lubricant is lower than the viscosity of the layer and the surface tension is negligible, linear stability analysis predicts that the interface is unstable regardless of the ratio of the thicknesses of the two layers (Loewenherz & Lawrence 1989). This behaviour has been characteristically described as 'anti-lubrication' (Chen 1990). A similar behaviour has been predicted for the three-layer film flow down an inclined plane or through a channel (e.g. Li 1969; Weinstein & Kurz 1991; Kliakhandler & Sivashinsky 1997).

One can make an analogy between the instability due to viscosity striation and the fingering Saffman–Taylor instability of an interface between two viscous fluids moving in a Hele–Shaw cell or through a porous medium. When the surface tension is sufficiently low, a low-viscosity fluid pushing a high-viscosity fluid is known to penetrate it by developing elongated fingers. But in the case of the fingering instability the motion can be modelled and analysed in the context of irrotational flow for the depth-averaged velocity, using a well-established formalism of vortex dynamics, and the instability may be attributed to the self-induced motion of an effective interfacial vortex sheet. An analogous formulation is not possible for two-dimensional viscous flow.

Instability due to a discontinuity in the viscous across an interface, or to the non-

uniform viscosity of a single fluid, has been studied from two general perspectives. From a fundamental point of view, one seeks to describe the motion of a sharp or diffuse interface in a general shear flow; from a practical point of view, one seeks to characterize the behaviour of liquid layers in channel or falling-film flow. The practical point of view is motivated by applications in two-phase flow through pipes and porous media, flooding in counter-current flows, co-extrusion of polymers, solvent cleaning, ink-jet printing, and physiological flows over tissues lined with coatings of biological materials.

There is yet another incentive for studying the dynamics of viscous interfacial flow, including the layered flow considered here, stemming from a long-standing desire to identify the physical mechanisms of heterogeneous mixing and describe the evolving morphology of the interfacial patterns due to agitation. Intricate interfacial patterns developing when passive interfaces – separating fluids with identical physical properties in the absence of surface tension – are subjected to, and advected by, various types of elementary flows have been described by experimental and numerical methods (e.g. Ottino 1989; Jana, Metcalfe & Ottino 1994). Much less work has been done on the motion of active interfaces separating fluids with different physical properties in the presence of surface tension. In this case, the velocity field may no longer be specified but is coupled with the dynamics of the flow, and the position and motion of the interface. Previous work has considered predominantly mixing in high-Reynolds-number and turbulent shear flows, such as shear layers and jets. The low-Reynolds-number viscosity-dominated or creeping motion has received much less attention.

Linear analyses of the stability of an interface between two immiscible viscous fluids in shearing motion have been presented on many occasions following the pioneering work of Yih (1967). The base flow may be an infinite shear flow, a semi-infinite shear flow bounded by a plane wall, a layered channel flow, or a multi-film flow. The motion may be driven by boundary translation, pressure drop, or a body force. Literature surveys can be found in the more recent papers of Renardy (1985), Yiantsios & Higgins (1988), Hooper (1989), Anturkar, Papanastasiou & Wilkes (1990), Su & Khomami (1992), Tilley, Davis & Bankoff (1994*a*), and Coward *et al.* (1997). Chapter 8 of a monograph by Han (1981) discusses the linear stability of layered non-Newtonian flow with reference to polymer processing.

Hesla, Pranckh & Preziosi (1986) devised a generalized Squire transformation that appears to make the study of three-dimensional perturbations redundant. They argued that, in the case of two-layer flow in a horizontal channel with constant surface tension and stable density stratification, only two-dimensional perturbations need to be considered in order to determine the marginal stability boundaries. Yiantsios & Higgins (1988) pointed out that, in some instances, the existence of the generalized Squire transformation does not necessarily render the study of three-dimensional perturbations redundant. The relation between three-dimensional and two-dimensional disturbances was discussed further and clarified by Joseph & Renardy (1992, vol. 1) and Tilley *et al.* (1994*a*).

Several attempts have been made to describe the nonlinear motion in the contexts of lubrication flow and weakly nonlinear theory of dynamical systems. For example, Hooper & Grimshaw (1985), Hooper (1985), Shlang *et al.* (1985), Renardy & Renardy (1993), and Charru & Fabre (1994) derived nonlinear evolution equations for the layer thicknesses in the limit as both the wavelength and amplitude of the perturbation are small compared to the unperturbed layer thickness. Ooms *et al.* (1985), and Tilley, Davis & Bankoff (1994*b*) derived more involved evolution equations applicable under general circumstances where the wavelength of the perturbation is small compared to

the unperturbed layer thickness, but the amplitude of the interface is not necessarily small compared to the channel width. These analyses and accompanying numerical solutions revealed behaviours similar to, but richer than, those exhibited by the widely studied single-film flow down an inclined plane. The physical relevance of these motions was criticized by Barthelet, Charru & Fable (1995). The lubrication-flow model of Ooms *et al*. (1985) will be discussed in §3 of the present paper.

The fully nonlinear motion has been the subject of several recent numerical studies. Bai, Kelkar & Joseph (1996) computed the shape of steadily propagating axisymmetric interfacial waves in the arrangement of core–annular flow, under the assumption that the core-fluid viscosity is so large that the core translates as a rigid body. The core–annular flow bears many similarities to the layered channel flow, but there are also important differences due to the destabilizing effect of surface tension in axisymmetric or three-dimensional flow. Coward *et al*. (1997) presented numerical simulations of two-layer plane-Couette flow at moderately high and relatively low Reynolds numbers using the volume-of-fluid method. Their results confirmed the destabilizing influence of the fluid inertia, and confirmed interfacial steepening due to nonlinearity. Similar numerical results for selected case studies were presented by Yiu & Chen (1996) and Zaleski *et al*. (1996). A systematic numerical investigation of the long-time evolution of two-layer Couette or Poiseuille flow has not been presented even under conditions of creeping flow.

Experimental studies of two-layer flow are also limited. Kao & Park (1972) established critical conditions for the onset of instabilities in turbulent two-layer Poiseuille flow in a rectangular channel; their results were discussed critically by Yiantsios & Higgins (1988). Han (1991, Chap. 8) discusses observations of three-dimensional instabilities of layered non-Newtonian flow and emphasizes their importance for product quality. It appears that the only experimental study of Couette flow is due to Barthelet *et al*. (1995). They found that, above a critical shear rate, the interface develops a fundamental slowly growing long wave, whose wavelength is equal to the perimeter of their square channel, and its harmonics. The dynamical properties of these waves were analysed in the context of the theory of dynamical systems.

In this work, we perform a numerical investigation of two-layer channel Stokes flow subject to two-dimensional perturbations, and examine the effect of the various geometrical or physical parameters of the flow. The motion is driven either by the translation of the walls or by a pressure gradient. In both cases, linear stability analysis predicts that the interfacial waves are neutrally stable or decay; neutral stability occurs only in the absence of surface tension. We compute the evolution of the interface when the magnitude of a disturbance is so large so that nonlinear effects may no longer be neglected, and the shape of the interface does not have a wavy form. The results reveal that, in both cases, the nonlinear motion can be unstable if the magnitude of the perturbation is sufficiently high. The morphology of the interfacial patterns emerging as a result of the instability is shown to depend strongly on the ratio of the viscosities of the two fluids.

The numerical investigations are conducted using a boundary integral method for periodic two-layer channel flow. In §2, we formulate the integral equations whose solutions produce the interfacial velocity for shear-driven, pressure-driven, and gravity-driven flow; the third case is included for completeness. The use of the periodic Green's function of the equations of Stokes flow in a channel that is bounded by two walls allows us to obtain accurate numerical results with a computational cost that ranges from reasonable to substantial but affordable.

2. Boundary integral formulation for channel flow

We consider the flow of two stratified fluids in a channel that is confined between two parallel plane walls located at $y = \pm h$, as shown in figure 1(*a*). The lower and upper fluids are labelled respectively with the superscript or subscript 1 and 2. The interfacial shape and velocity field are repeated along the x-axis with period L, and the pressure is allowed to drop by a specified amount over the length of each periodic cell.

Assuming that the appropriate Reynolds number of the flow is negligibly small so that the effects of inertia can be uniformly neglected and the motion of both fluids is governed by the equations of Stokes flow, we set out to develop a boundary-integral formulation that is applicable to the three modular cases of shear-driven, pressure-driven, and gravity-driven Stokes flow, or any combination thereof. The ultimate objective is to derive integral equations for the interfacial velocity that can be solved with the least amount of effort and a high level of accuracy.

2.1. *General formulation*

As a preliminary, we decompose the velocity fields of the lower and upper fluids, denoted as $\boldsymbol{u}^{(1)}$ and $\boldsymbol{u}^{(2)}$, into a reference component, denoted as $\boldsymbol{y}^{R(1)}$ and $\boldsymbol{u}^{R(2)}$, and a disturbance component, denoted as $\boldsymbol{u}^{D(1)}$ and $\boldsymbol{u}^{D(2)}$. Thus, by definition

$$\boldsymbol{u}^{(1)} = \boldsymbol{u}^{R(1)} + \boldsymbol{u}^{D(1)}, \quad \boldsymbol{u}^{(2)} = \boldsymbol{u}^{R(2)} + \boldsymbol{u}^{D(2)}. \tag{1}$$

The reference components satisfy the continuity equation and the Stokes equation with the body-force term included,

$$-\boldsymbol{\nabla} p^{R(1)} + \mu_1 \nabla^2 \boldsymbol{u}^{R(1)} + \rho_1 \boldsymbol{g} = \boldsymbol{0}, \quad -\boldsymbol{\nabla} p^{R(2)} + \mu_2 \nabla^2 \boldsymbol{u}^{R(2)} + \rho_2 \boldsymbol{g} = \boldsymbol{0}, \tag{2}$$

where p is the pressure, ρ is the density, and $\boldsymbol{g}$ is the acceleration due to gravity. The disturbance components satisfy the continuity equation and the homogeneous Stokes equation,

$$-\boldsymbol{\nabla} p^{D(1)} + \mu_1 \nabla^2 \boldsymbol{u}^{D(1)} = \boldsymbol{0}, \quad -\boldsymbol{\nabla} p^{D(2)} + \mu_2 \nabla^2 \boldsymbol{u}^{D(2)} = \boldsymbol{0}. \tag{3}$$

All velocity fields satisfy the continuity equation. The boundary conditions imposed on the reference and disturbance flows will be discussed later in this section.

Requiring the velocity to be continuous across the interface, we find that at a point $\boldsymbol{x}$ located at the interface,

$$\boldsymbol{u}^{R(1)}(\boldsymbol{x}) + \boldsymbol{u}^{D(1)}(\boldsymbol{x}) = \boldsymbol{u}^{R(2)}(\boldsymbol{x}) + \boldsymbol{u}^{D(2)}(\boldsymbol{x}). \tag{4}$$

The jump in the traction across the interface, defined as $\Delta \boldsymbol{f} \equiv \boldsymbol{f}^{(1)} - \boldsymbol{f}^{(2)} = (\boldsymbol{\sigma}^{(1)} - \boldsymbol{\sigma}^{(2)}) \cdot \boldsymbol{n}$, due, for example, to surface tension, is also resolved into a reference and a disturbance component; $\boldsymbol{\sigma}$ is the stress tensor, and $\boldsymbol{n}$ is the unit vector normal to the interface pointing into the lower fluid labelled 1 as shown in figure 1(*a*). Thus, for a point $\boldsymbol{x}$ located at the interface, we write

$$\Delta \boldsymbol{f}(\boldsymbol{x}) = \Delta \boldsymbol{f}^{R}(\boldsymbol{x}) + \Delta \boldsymbol{f}^{D}(\boldsymbol{x}). \tag{5}$$

For an interface with uniform surface tension γ, $\Delta \boldsymbol{f}(z) = \gamma \kappa \boldsymbol{n}$, where κ is the curvature of the trace of the interface in the (x, y)-plane.

To complete the preparations for the boundary-integral formulation, we introduce the periodic Green's function of two-dimensional channel Stokes flow, denoted as $\boldsymbol{G}^{1P-2W}(\boldsymbol{x}, \boldsymbol{x}_0; \alpha)$, where the superscripts $1P$ and $2W$ stand, respectively, for *singly periodic* and *two walls*. Physically, $u_i(\boldsymbol{x}) = 1/(4\pi\mu)\, G_{ij}^{1P-2W}(\boldsymbol{x}, \boldsymbol{x}_0; \alpha)\, b_j$ is the velocity at the point $\boldsymbol{x}$ induced by an array of point forces with equal strengths $\boldsymbol{b}$ deployed along the x-axis and separated by a distance L, where one of the point forces is located at the point $\boldsymbol{x}_0$; μ is the density of the fluid. The parameter α sets the pressure drop over one period of the flow, ΔP^{1P-2W}, and thus the axial flow rate Q^{1P-2W}: a two-dimensional

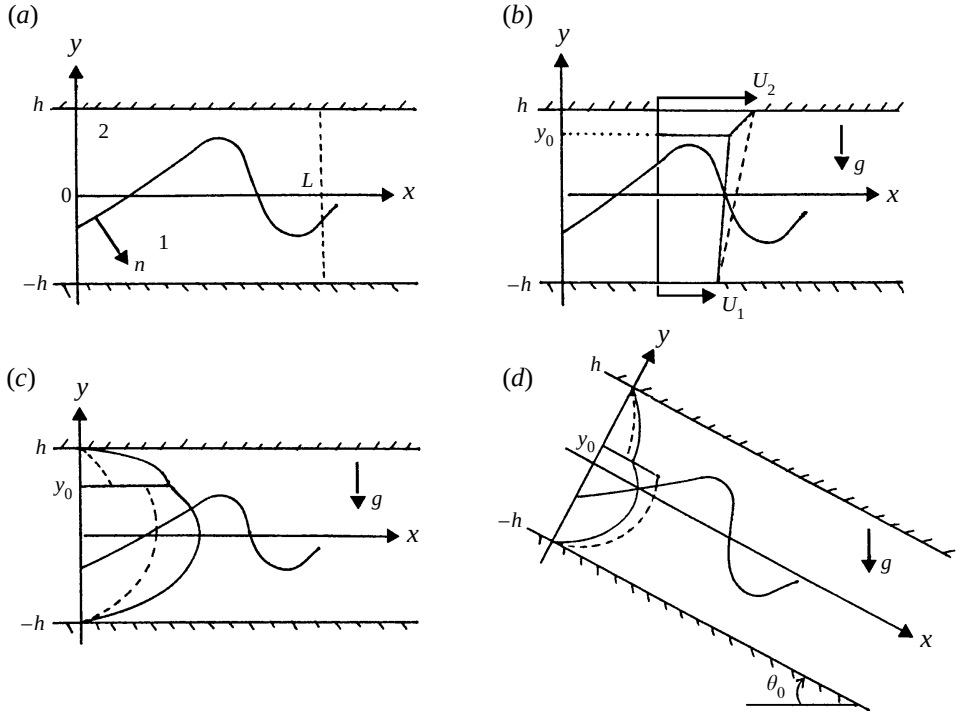

FIGURE 1. (*a*) Periodic two-layer flow in a channel confined between two parallel plane walls. (*b*) Couette flow driven by the translation of the two walls. (*c*) Poiseuille flow driven by a pressure gradient. (*d*) Gravity-driven flow in an inclined channel.

Hagen–Poiseuille flow may be added to the flow produced by the point forces to alter both. The computation of $\boldsymbol{G}^{1P-2W}(\boldsymbol{x},\boldsymbol{x}_0;\alpha)$, ΔP^{1P-2W}, and Q^{1P-2W}, and of the associated stress tensor $\boldsymbol{T}^{1P-2W}(\boldsymbol{x},\boldsymbol{x}_0;\alpha)$ are discussed in detail by Pozrikidis (1992) and Zhou & Pozrikidis (1993). A FORTRAN subroutine that computes these quantities is available from the author.

We are now in a position to apply the well-established boundary-integral formulation for interfacial flow, e.g. Pozrikidis (1992, Chap. 5), to describe and subsequently compute the disturbance flow. Stipulating that the disturbance velocity vanishes over the upper and lower channel walls, taking into account equations (4) and (5), and using the distinctive properties of the Green's function, we express the disturbance velocity in terms of integrals evaluated over one period of the interface, denoted as I. For a point $\boldsymbol{x}_0$ that lies within the lower fluid, labelled 1, we find

$$
\begin{aligned}
u_j^{D(1)}(\boldsymbol{x}_0) = {} & \frac{1}{4\pi\mu_1} Q^{1P-2W}\,\Delta P^D \boldsymbol{i} - \frac{1}{4\pi\mu_1}\int_I (\Delta f_i - \Delta f_i^R)(\boldsymbol{x})\, G_{ij}^{1P-2W}(\boldsymbol{x},\boldsymbol{x}_0;\alpha)\,\mathrm{d}l(\boldsymbol{x}) \\
& + \frac{1-\lambda}{4\pi}\int_I u_i^{D(1)}(\boldsymbol{x})\, T_{ijk}^{1P-2W}(\boldsymbol{x},\boldsymbol{x}_0;\alpha)\, n_k(\boldsymbol{x})\,\mathrm{d}l(\boldsymbol{x}) \\
& - \frac{\lambda}{4\pi}\int_I (u_i^{R(1)} - u_i^{R(2)})(\boldsymbol{x})\, T_{ijk}^{1P-2W}(\boldsymbol{x},\boldsymbol{x}_0;\alpha)\, n_k(\boldsymbol{x})\,\mathrm{d}l(\boldsymbol{x}) \\
& - \frac{1}{4\pi}[Q^{D(1)} + \lambda Q^{D(2)}]\,\Delta P^{1P-2W}\boldsymbol{i},
\end{aligned}
\tag{6}
$$

where ΔP^D is the pressure drop due to the disturbance flow over one period, $Q^{D(1)}$ and

$Q^{D(2)}$ are the axial flow rates of the lower and upper fluid into or out of a periodic cell containing the periodic interfacial segment I, $\boldsymbol{i}$ is the unit vector along the x-axis, and $\lambda = \mu_2/\mu_1$.

Considering a point $\boldsymbol{x}_0$ that lies within the upper fluid, labelled 2, we derive an identical expression, except that the velocity on the left-hand side is multiplied by the viscosity ratio λ. For a point $\boldsymbol{x}_0$ that lies at the interface I, the velocity on the left-hand side is multiplied by the factor $(1+\lambda)/2$, and the second and third integrals on the right-hand side are interpreted in the sense of their principal value; this is an integral equation of the second kind for the disturbance interfacial velocity $\boldsymbol{u}^{D(1)}(\boldsymbol{x})$.

To expedite the numerical solution, we stipulate that $\Delta P^{1P-2W} = 0$, for then the troublesome last term on the right-hand side of equation (6) disappears. This choice will be indicated by setting $\alpha = 0$ in the argument of the Green's function. Furthermore, we specify that $\Delta P^D = 0$, for then the first term on the right-hand side of equation (6) disappears and we are left with a simplified expression. These two assumptions will be implicit in the forthcoming discussion. It is sometimes, but not always, beneficial to choose a reference velocity field that is continuous across the interface, for then the third integral on the right-hand side of equation (6) disappears leading to a simplified representation; in this case, $\boldsymbol{u}^{D(1)}(\boldsymbol{x}) = \boldsymbol{u}^{D(2)}(\boldsymbol{x})$ at a point $\boldsymbol{x}$ that is located at the interface.

In the following three subsections, we derive specific forms of the boundary-integral representation and associated integral equation emanating from the master equation (6), for the three fundamental modes of shear-driven, pressure-driven, and gravity-driven flow. These forms are distinguished by the choice of the reference flows.

2.2. *Shear-driven flow*

Consider shear-driven flow in a horizontal channel of width $2h$, as depicted in figure 1(*b*). The lower and upper walls translate parallel to themselves with respective velocities equal to U_1 and U_2. The origin of the coordinate system has been set midway between the two plates, and the gravity vector points toward the negative direction of the y-axis.

In this case, it is beneficial to select the reference velocity and pressure fields

$$\left.\begin{aligned} \boldsymbol{u}^{R(1)} &= \chi(y-y_R)\,\boldsymbol{i}, \quad p^{R(1)} = P_0 - \rho_1 g y, \\ \boldsymbol{u}^{R(2)} &= \chi(y-y_R)\,\boldsymbol{i}, \quad p^{R(2)} = P_0 - \rho_2 g y, \end{aligned}\right\} \tag{7}$$

where χ is a global shear rate and y_R is a reference length, both to be defined shortly, P_0 is a reference pressure, and g is the magnitude of the acceleration due to gravity. Note that this reference velocity field is continuous across the interface. One may readily verify that the fields (7) satisfy equations (2).

To find the appropriate values of χ and y_R, we recall that the disturbance velocity should vanish at the two walls, and require that $u^{R(1)}(y=-h) = -\chi(h+y_R) = U_1$, and $u^{R(2)}(y=h) = \chi(h-y_R) = U_2$, where u signifies the x-component of the velocity. We then find

$$\chi = \frac{\Delta U}{2h}, \quad y_R = -h\frac{U_1+U_2}{\Delta U}, \tag{8}$$

where $\Delta U = U_2 - U_1$. The linear profile of the reference velocity is drawn with the dashed line in figure 1(*b*).

With the choices stated in (7), the boundary-integral representation (6) simplifies to

$$u_j^{D(1)}(\boldsymbol{x}_0) = -\frac{1}{4\pi\mu_1}\int_I (\Delta f_i - \Delta f_i^R)(\boldsymbol{x})\, G_{ij}^{1P-2W}(\boldsymbol{x},\boldsymbol{x}_0;\alpha=0)\,\mathrm{d}l(\boldsymbol{x}) + \frac{1-\lambda}{4\pi}\int_I u_i^D(\boldsymbol{x})\, T_{ijk}^{1P-2W}(\boldsymbol{x},\boldsymbol{x}_0;\alpha=0)\, n_k(\boldsymbol{x})\,\mathrm{d}l(\boldsymbol{x}), \quad (9)$$

and the associated integral equation is

$$u_j^D(\boldsymbol{x}_0) = -\frac{1}{4\pi\mu_1}\frac{2}{1+\lambda}\int_I (\Delta f_i - \Delta f_i^R)(\boldsymbol{x})\, G_{ij}^{1P-2W}(\boldsymbol{x},\boldsymbol{x}_0;\alpha=0)\,\mathrm{d}l(\boldsymbol{x}) + \frac{1-\lambda}{4\pi}\frac{2}{1+\lambda}\int_I{}^{\mathrm{PV}} u_i^D(\boldsymbol{x})\, T_{ijk}^{1P-2W}(\boldsymbol{x},\boldsymbol{x}_0;\alpha=0)\, n_k(\boldsymbol{x})\,\mathrm{d}l(\boldsymbol{x}), \quad (10)$$

where the point $\boldsymbol{x}_0$ lies on the interface. The qualifier PV designates the principal value of the double-layer integral. Note that the coefficient of the double-layer integral vanishes when $\lambda = 1$.

A straightforward computation shows that the jump in the interfacial traction appearing in the single-layer integral on the right-hand sides of (9) and (10) is given by

$$\Delta\boldsymbol{f}^R \equiv \boldsymbol{f}^{R(1)} - \boldsymbol{f}^{R(2)} = (\boldsymbol{\sigma}^{R(1)} - \boldsymbol{\sigma}^{R(2)})\cdot\boldsymbol{n} = (1-\lambda)\,\mu_1\,\chi(n_y\,\boldsymbol{i} + n_x\boldsymbol{j}) + \Delta\rho\, gy\boldsymbol{n}, \quad (11)$$

where $\Delta\rho = \rho_1 - \rho_2$, and $\boldsymbol{j}$ is the unit vector along the y-axis.

In the simple case of rectilinear flow with a flat interface located at $y = y_0$, an exact solution to the integral equation (10) can be found by elementary methods. In this case, the x-components of the velocities of the lower and upper fluids are given respectively by

$$u^{(1)} = \xi_1(y+h) + U_1, \quad u^{(2)} = \xi_2(y-h) + U_2, \quad (12)$$

where

$$\xi_1 = \frac{\Delta U}{h_1}\frac{\lambda}{\lambda+R}, \quad \xi_2 = \frac{\Delta U}{h_1}\frac{1}{\lambda+R}, \quad (13)$$

$h_1 = h + y_0$ is the lower-layer thickness, $h_2 = h - y_0$ is the upper-layer thickness, and R is the thickness ratio, $R = h_2/h_1$. This composite velocity profile is drawn with the solid line in figure 1(*b*). The velocity at the interface is given by $u_I = \Delta U\lambda/(\lambda+R) + U_1$. Combining this expression with (7) and (8), we find that the disturbance velocity at the interface is given by

$$u_I^D = \Delta U\frac{R}{1+R}\frac{\lambda-1}{\lambda+R}. \quad (14)$$

This is an exact solution of the integral equation (10) for a flat interface with $\Delta\boldsymbol{f} = c\boldsymbol{n}$ where c is an arbitrary constant, and for any period length L.

2.3. *Pressure-driven flow*

We consider next pressure-driven flow in a horizontal channel with a non-zero pressure drop over one period, equal to ΔP, corresponding to the effective pressure gradient $G = -\Delta P/L$, as depicted in figure 1(*c*).

In this case, we select the reference velocity and pressure fields

$$\left.\begin{aligned} \boldsymbol{u}^{R(1)} &= \frac{G}{2\mu_1}(h^2 - y^2)\,\boldsymbol{i}, \quad p^{R(1)} = P_1 - Gx - \rho_1 gy, \\ \boldsymbol{u}^{R(2)} &= \frac{G}{2\mu_2}(h^2 - y^2)\,\boldsymbol{i}, \quad p^{R(2)} = P_2 - Gx - \rho_2 gy, \end{aligned}\right\} \quad (15)$$

where P_1 and P_2 are two reference pressures. Note that this reference velocity, whose profile is drawn with the dashed line in figure 1(*c*), is not continuous across the interface. One may readily verify that the fields (15) satisfy (2), as required. The associated jump in the interfacial traction is

$$\Delta \boldsymbol{f}^R = \Delta\rho\, g y \boldsymbol{n} - (P_1 - P_2)\,\boldsymbol{n}. \tag{16}$$

Substituting these expressions into the boundary-integral representation (6), noting that at the interface $\boldsymbol{u}^{R(2)} = (1/\lambda)\,\boldsymbol{u}^{R(1)}$, combining the third with the second integral on the right-hand side, and adding to both sides the reference velocity $\boldsymbol{u}^{R(1)}$, we obtain a simplified expression for the velocity in fluid 1:

$$u_j^{(1)}(\boldsymbol{x}_0) = u_j^{R(1)}(\boldsymbol{x}_0) - \frac{1}{4\pi\mu_1}\int_I (\Delta f_i - \Delta f_i^R)(\boldsymbol{x})\, G_{ij}^{1P-2W}(\boldsymbol{x}, \boldsymbol{x}_0; \alpha = 0)\, \mathrm{d}l(\boldsymbol{x}) + \frac{1-\lambda}{4\pi}\int_I u_i(\boldsymbol{x})\, T_{ijk}^{1P-2W}(\boldsymbol{x}, \boldsymbol{x}_0; \alpha = 0)\, n_k(\boldsymbol{x})\, \mathrm{d}l(\boldsymbol{x}). \tag{17}$$

The associated integral equation for the interfacial velocity is

$$u_j(\boldsymbol{x}_0) = \frac{2}{1+\lambda} u_j^{R(1)}(\boldsymbol{x}_0) - \frac{1}{4\pi\mu_1}\frac{2}{1+\lambda}\int_I (\Delta f_i - \Delta f_i^R)(\boldsymbol{x})\, G_{ij}^{1P-2W}(\boldsymbol{x}, \boldsymbol{x}_0; \alpha = 0)\, \mathrm{d}l(\boldsymbol{x}) + \frac{1-\lambda}{4\pi}\frac{2}{1+\lambda}\int_I^{\mathrm{PV}} u_i(\boldsymbol{x})\, T_{ijk}^{1P-2W}(\boldsymbol{x}, \boldsymbol{x}_0; \alpha = 0)\, n_k(\boldsymbol{x})\, \mathrm{d}l(\boldsymbol{x}) \tag{18}$$

where the point $\boldsymbol{x}_0$ lies at the interface.

In the simple case of rectilinear flow with a flat interface located at $y = y_0$, an exact solution to the integral equation (18) can be found by elementary methods. Using the notation of §2.2, we find that the x-component of the velocity of the lower and upper fluid is given respectively by

$$u^{(1)} = (y/h + 1)(\psi_1 y + u_I), \quad u^{(2)} = (y/h - 1)(\psi_2 y - u_I), \tag{19}$$

where ψ_1 and ψ_2 are two shear rates, and u_I is the velocity at the interface given by

$$u_I = \frac{Gh^2}{\mu_1}\frac{1}{1+R}\frac{2R}{\lambda+R}, \tag{20}$$

where $R = h_2/h_1$. This composite velocity profile is drawn with the solid line in figure 1(*c*). The right-hand side of (20) satisfies the integral equation (18) with $\Delta\boldsymbol{f} = c\boldsymbol{n}$ where c is an arbitrary constant, for a flat interface, and for any period length L.

2.4. *Gravity-driven flow*

In the final case, we consider gravity-driven flow in a channel that is inclined at an angle θ_0 with respect to the horizontal direction. The channel is assumed to be open at both ends so that there is no pressure drop across its length, as depicted in figure 1(*d*).

In this case, we select the reference velocity and pressure fields

$$\left.\begin{aligned} \boldsymbol{u}^{R(1)} &= \frac{\rho_1 g \sin\theta_0}{2\mu_1}(h^2 - y^2)\,\boldsymbol{i}, \quad p^{R(1)} = P_1 - \rho_1 g y \sin\theta_0, \\ \boldsymbol{u}^{R(2)} &= \frac{\rho_2 g \sin\theta_0}{2\mu_2}(h^2 - y^2)\,\boldsymbol{i}, \quad p^{R(2)} = P_2 - \rho_2 g y \sin\theta_0, \end{aligned}\right\} \tag{21}$$

where P_1 and P_2 are two reference pressures. As in the case of pressure-driven flow, the reference velocity is not continuous across the interface. One may readily verify that the fields (21) satisfy (2), as required. The associated jump in the interfacial traction is

$$\Delta \boldsymbol{f}^R = \Delta\rho\, g y \begin{bmatrix} n_x \cos\theta_0 - n_y \sin\theta_0 \\ -n_x \sin\theta_0 + n_y \cos\theta_0 \end{bmatrix} - (P_1 - P_2)\,\boldsymbol{n}. \tag{22}$$

Substituting these expressions into the boundary-integral representation (6), and combining several terms, we obtain

$$u_j^{(1)}(\boldsymbol{x}_0) = u_j^{R(1)}(\boldsymbol{x}_0) - \frac{1}{4\pi\mu_1}\int_I (\Delta f_i - \Delta f_i^R)(\boldsymbol{x})\, G_{ij}^{1P-2W}(\boldsymbol{x}, \boldsymbol{x}_0; \alpha = 0)\, \mathrm{d}l(\boldsymbol{x})$$

$$+ \frac{1}{4\pi}\int_I [(1-\lambda)\, u_i(\boldsymbol{x}) - (1-\beta)\, u_i^{R(1)}(\boldsymbol{x})]\, T_{ijk}^{1P-2W}(\boldsymbol{x}, \boldsymbol{x}_0; \alpha = 0)\, n_k(\boldsymbol{x})\, \mathrm{d}l(\boldsymbol{x}), \tag{23}$$

where we have introduced the density ratio $\beta = \rho_2/\rho_1$.

The associated integral equation for the interfacial velocity $\boldsymbol{u}$ is

$$u_j(\boldsymbol{x}_0) = \frac{1+\beta}{1+\lambda} u_j^{R(1)}(\boldsymbol{x}_0) - \frac{1}{4\pi\mu_1}\frac{2}{1+\lambda}\int_I (\Delta f_i - \Delta f_i^R)(\boldsymbol{x})\, G_{ij}^{1P-2W}(\boldsymbol{x}, \boldsymbol{x}_0; \alpha = 0)\, \mathrm{d}l(\boldsymbol{x})$$

$$+ \frac{1}{2\pi}\frac{1}{1+\lambda}\int_I^{\mathrm{PV}} [(1-\lambda)\, u_i(\boldsymbol{x}) - (1-\beta)\, u_i^{R(1)}(\boldsymbol{x})]\, T_{ijk}^{1P-2W}(\boldsymbol{x}, \boldsymbol{x}_0; \alpha = 0)\, n_k(\boldsymbol{x})\, \mathrm{d}l(\boldsymbol{x}), \tag{24}$$

where the point $\boldsymbol{x}_0$ lies at the interface. Note that the disappearance of the double-layer potential requires that the physical properties of the two fluids be matched, $\lambda = 1$ and $\beta = 1$.

In the simple case of rectilinear flow with a flat interface located at $y = y_0$, an exact solution to the integral equation (24) can be found by elementary methods. The composite velocity profile is drawn with the solid line in figure 1(*d*). The x-component of the interfacial velocity is given by

$$u_I = \frac{\rho_1 g h^2 \sin\theta_0}{\mu_1}\frac{1+\beta R}{(1+R)^2}\frac{2R}{\lambda + R}. \tag{25}$$

When $\beta = 1$, (23), (24), and (25) reduce, respectively, to (17), (18), and (20) for pressure-driven flow with an effective pressure gradient given by $G = \rho_1 g \sin\theta_0$.

2.5. *Numerical solution of the integral equations*

The integral equations of the second kind derived in the preceding subsections were solved using a standard iterative method. One period of the interface was traced by a set of marker points, and the interfacial velocity was assumed to vary linearly with respect to arclength between two adjacent points. The theoretical foundation of the iterative method and its numerical implementation are well-established (e.g. Pozrikidis 1992) and will not be described here. The accuracy of the numerical method was confirmed by comparing the numerical solution to the exact solutions for the flat interfaces discussed previously in this section, and finding agreement up to the sixth significant figure, as well as by performing numerous tests of convergence.

To describe the evolution of the interface, the position of each marker point was advanced using either the component of the velocity of the fluid normal to the interface, or the total velocity of the fluid. The integration of the associated system of

ordinary differential equations for the marker point position was carried out using the second-order Runge–Kutta method. An adaptive point redistribution routine was implemented to allow the resolution of regions of high curvature, while keeping the number of marker points at an economical level. The change in the area of each layer due to numerical error was less than 0.1 % throughout the duration of each simulation, and much less than that in most cases.

In a typical simulation, each period of each interface was described by 32 to 120 marker points. The computational cost was a strong function of the number of marker points and flow conditions, as will be discussed in the following sections, demanding from 1 to 60 h of CPU time on a SUN SPARCstation 20. The case $\lambda = 1$ was given particular attention since then the integral equation reduces to an integral representation, and the computation of the interfacial velocity incurs the least computational cost.

3. Shear-driven flow

First, we study the stability of the interface between two layers in shear-driven Stokes flow depicted in figure 1 (*b*), subject to a two-dimensional periodic perturbation of wavelength L that disturbs the interface in a sinusoidal manner with amplitude a_0. The densities of the fluids are assumed to be matched so that gravity does not play a role; in the notation of the preceding section, $\beta = 1$. More formally, we assume that a properly defined Bond or Weber number of the flow is infinitely large. Furthermore, we stipulate that the perturbation does not generate a pressure drop across each period; physically, the channel is open to the atmosphere or to a constant-pressure chamber at both ends.

The motion of the interface depends on the viscosities of the two fluids μ_1 and μ_2, the interfacial tension γ, the unperturbed thicknesses of the two layers h_1 and h_2, the velocities of the two walls U_1 and U_2, and the wavelength and amplitude of the perturbation L and a_0. A number of alternative sets of dimensionless parameters can be formed using these variables; the appropriate choice depends on the objective of the investigation.

If the objective is to study the behaviour of an interface between two viscous fluids in a flow that can be locally approximated as a simple shear flow, it is appropriate to reduce all lengths by the wavelength L, time by the shear rate of the lower fluid evaluated at the unperturbed interface ξ_1 defined in (13), and stresses by $\mu_1 \xi_1$, and introduce the capillary number $Ca_1 = \mu_1 \xi_1 L/\gamma$. The four dimensionless numbers characterizing the flow are Ca_1, $\lambda = \mu_2/\mu_1$, $R = h_2/h_1$, h/L, and a_0/L. An alternative set of dimensionless numbers would be $Ca_2 = \mu_2 \xi_2 L/\gamma$, λ, R, h/L, and a_0/L.

If, on the other hand, the objective is to study the behaviour of layered flow in a channel of specified dimensions when varying the properties of the fluids, it is appropriate to reduce all lengths by the channel semi-width h, time by the shear rate $\chi = \Delta U/(2h)$, and stresses by $\mu_1 \chi$, and introduce the capillary number $Ca = \mu_1 \chi h/\gamma$. The four dimensionless numbers of the flow are Ca, λ, R, L/h, and a_0/h.

In the numerical studies to be described in the remainder of this section, we perform the second type of parametric investigation, but we re-interpret the results on occasion within the first framework. To reduce the parametric space, we set $R = 1$, that is we consider layers of equal thickness; the effect of layer thickness will be discussed in the concluding section. The figures will depict the evolution of the interface in a frame of reference that moves with the average velocity of the two plates $\Delta U/2$.

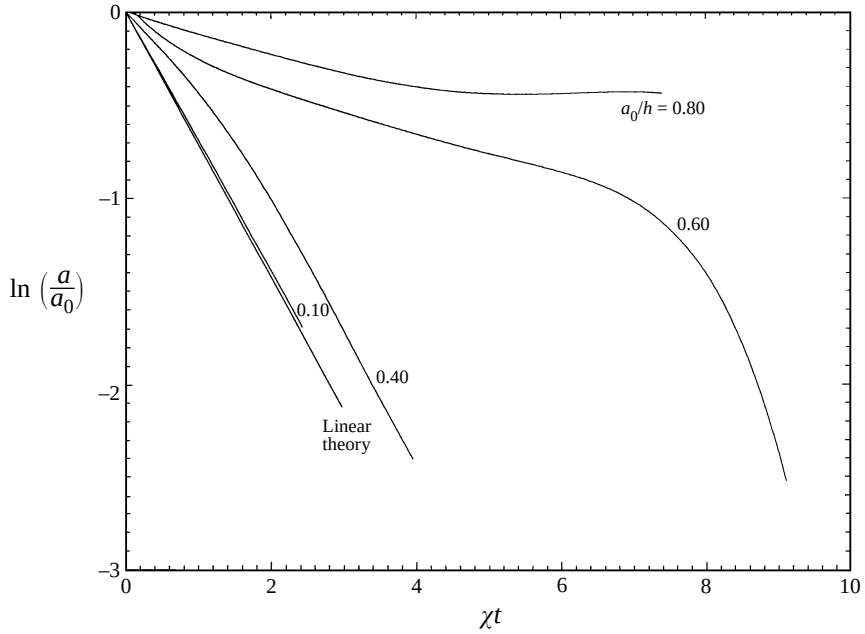

FIGURE 2. Evolution of the maximum height of the interface for two layers of equal thickness, $R = 1$, fluids of equal viscosity, $\lambda = 1$, equal density, $\beta = 1$, $Ca = 1$, reduced wavelength $L/h = 2$, and perturbations of different initial amplitudes. The straight line represents the predictions of the linear theory.

3.1. *Linear theory*

Linear theory predicts that, as long as both a_0/h and a_0/L are sufficiently small, a sinusoidal perturbation decays for any finite value of the capillary number, that is, as long as the surface tension is non-zero. The interfacial wave is described by the equation

$$y = y_0 + A(t)\cos(2\pi(x - c_P t)/L), \tag{26}$$

where

$$A(t) = a_0 \exp(\sigma_I t) \tag{27}$$

is the instantaneous amplitude of the perturbation, σ_I is the growth rate, and c_P is the phase velocity. Relations between c_P, σ_I and the various geometrical and physical variables of the flow may be derived in closed form by carrying out a standard linear analysis (e.g. Pozrikidis 1997*a*, Chap. 9). But the intermediate and final expressions are lengthy, and are not presented. A FORTRAN program that produces these quantities can be obtained from the author on request.

3.2. *Fluids of equal viscosity*

First, we investigate the effect of the reduced amplitude of the perturbation a_0/h and of the capillary number $Ca = \mu_1 \chi h/\gamma$, with reference to the flow of two layers of equal thickness, $R = 1$, for fluids of equal viscosity, $\lambda = 1$, and for reduced wavelength $L/h = 2$.

For $a_0/h = 0.10$ and $Ca = 1$, the numerical results are in excellent agreement with the predictions of the linear theory. In figure 2, we plot, on a log-linear scale, the ratio $a(t)/a_0$, where $a(t)$ is the maximum amplitude of the interface computed by quadratic interpolation, and obtain a nearly straight line corresponding to exponential decay. The predictions of the linear theory are represented by the straight line of slope -0.70795.

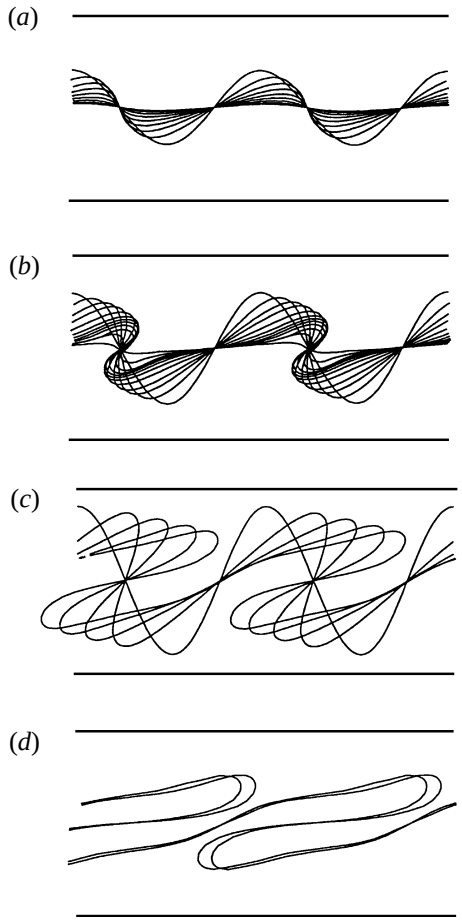

FIGURE 3. Sequences of interfacial profiles for $R = 1$, $\lambda = 1$, $\beta = 1$, $Ca = 1$, $L/h = 2$, and initial amplitude (*a*) $a_0/h = 0.40$ at $t^* = t\Delta U/h = 0$, 0.5, 1.0, 2.0, 2.5, 3.0, 3.5, 4.0; (*b*) $a_0/h = 0.60$ at $t^* = 0$, 0.4, 0.8, 1.2, 2.0, 3.0, 4.0, 5.0, 6.0, 7.0, 8.0, 9.0; (*c*, *d*) $a_0/h = 0.80$ at (*c*) $t^* = 0$, 0.8, 1.6, 2.7, 4.0; (*d*) $t^* = 6.0$, 7.4.

For the even smaller amplitude $a_0/h = 0.001$ and $Ca = 1$, the rate of decay extracted from the numerical results agrees with the analytical prediction to the third significant figure.

In figure 3(*a*), we present a sequence of instantaneous interfacial profiles for a disturbance with a large initial amplitude $a_0/h = 0.40$ and $Ca = 1$. The perturbation decays, but examining the corresponding curve in figure 2 shows that the initial rate of decay is substantially lower than that predicted by the linear theory. Thus, finite-amplitude effects reduce the rate of decay of a perturbation. When the amplitude of the interface has become small, the rate of decay rises and approaches that predicted by the linear theory. Finite-amplitude effects are manifested in the shifting of the wave crests and troughs due to wave steepening under the action of the simple shear flow. Since the interface assumes a flat shape at long times, this perturbation is stable.

For $a_0/h = 0.60$, we observe a more interesting behaviour. The profiles illustrated in figure 3(*b*) show that the competition between the tendency of the interface to flatten due to surface tension, and the convective action of the simple shear flow, causes the formation of a periodic sequence of transient lobes. The folding and immediate

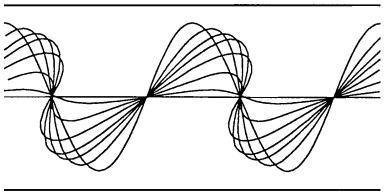

FIGURE 4. Sequences of interfacial profiles for $R = 1$, $\lambda = 1$, $\beta = 1$, $Ca = 2$, $L/h = 2$, and initial amplitude $a_0/h = 0.80$ at $t^* = 0$, 0.3, 0.6, 0.9, 1.8, 3.0, 4.0.

unfolding of the interfacial corrugations is a striking feature of this motion. Figure 2 shows that the initial rate of decay is much smaller than that predicted by the linear analysis, whereas the final rate of decay is somewhat higher than that predicted by linear analysis due to the steepening of the wave.

A large-amplitude perturbation with $a_0/h = 0.80$ can no longer be restrained by surface tension, as depicted in figure 3(*c*, *d*). The maximum height of the interface decreases monotonically in time, but the folding of the interface leads to the development of a sequence of permanent bulges that eventually transform into elongated drops. Figure 2 shows that the thickness of the interfacial layer where overturning occurs tends to a constant value at long times. The necks supporting the bulges keep thinning and possibly break up at a finite time yielding a series of compound drops. If the motion were three-dimensional, the necks would be threads, and the Rayleigh capillary instability would facilitate the breakup. The CPU time required for carrying out the computations shown in figure 3 ranges from 2 to 24 hours on the facilities described in §2.

For the conditions considered here, the critical amplitude of the perturbation above which the interface folds lies between $0.40h$ and $0.8h$. A rough estimate of this threshold can be obtained by comparing the magnitudes of the time it takes the interfacial wave to decay according to linear theory, τ_D, and the time it takes the crest of the wave to travel a distance equal to $L/4$ under the action of the unperturbed shear flow, τ_T, thereby generating a sigmoidal profile. Assuming that the amplitude of the wave has decayed to the value $a = 0.10L$ after the time period τ_D, and using (27), we find $-\tau_D \sigma_I = \ln(L/a_0) - 2.3$. Setting $\tau_T = L/(4\chi a_0)$, and assuming that the interface will fold when $\tau_D > \tau_T$, we derive a nonlinear algebraic equation for the critical amplitude:

$$\ln(L/a_{0,cr}) - (\sigma_I/4\chi)(L/a_{0,cr}) - 2.3 = 0. \tag{28}$$

Using the value $\sigma_I/\chi = -0.70795$, we find $a_{0,cr}/L = 4.50$ or $a_{0,cr}/h = 0.44$, which is consistent with the results of the numerical computation. A less conservative definition for τ_D would have given even better agreement.

Further numerical results confirm the physical intuition that increasing the surface tension raises the critical amplitude for the interface to suffer permanent deformation. For example, in figure 4, we present a sequence of profiles for a perturbation with $a_0/h = 0.8$ and $Ca = 2$. The interface tends to fold, but the restraining action of the surface tension eventually smooths out the corrugations, and the asymptotic shape of the interface at large times is flat. Solving (28) with $\sigma_I/\chi = -1.4159$ gives $a_0/L = 3.21$ corresponding to $a_0/h = 0.62$, which provides us with a conservative estimate for permanent deformation.

The preceding results correspond to reduced wavelength $L/h = 2$. Numerical experimentation showed that perturbations with smaller or larger wavelengths behave

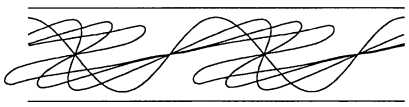

FIGURE 5. Sequences of interfacial profiles for $R = 1$, $\lambda = 1$, $\beta = 1$, $Ca = 1$, $L/h = 4$, and initial amplitude $a_0/h = 0.80$ at $t^* = 0$, 1.4, 3.0, 5.0.

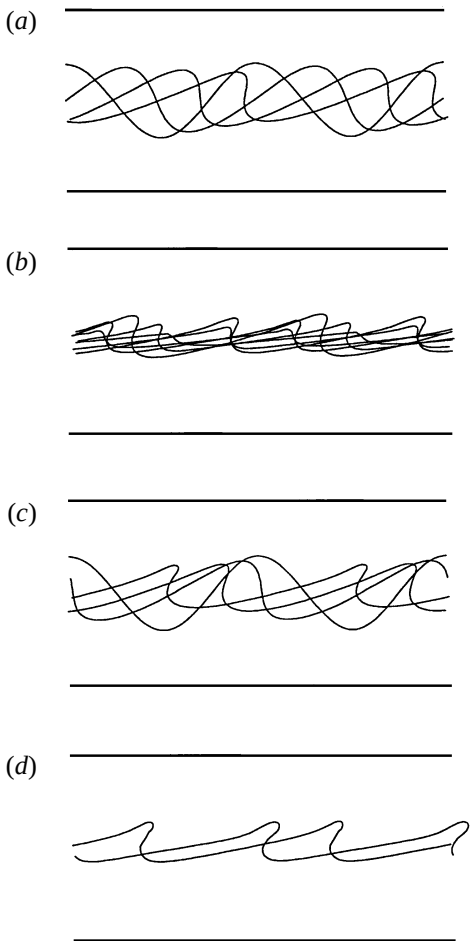

FIGURE 6. Sequences of interfacial profiles for $R = 1$, $\beta = 1$, $Ca = 1$, $L/h = 2$, and initial amplitude $a_0/h = 0.40$, for (a, b) $\lambda = 5$, at $t^* = 0$, 0.8, 1.6, 2.4, 3.6, 5.2, 6.2; (c, d) $\lambda = 10$, at $t^* = 0$, 2.1, 4.2, 6.0, 8.0, 9.6.

in a similar fashion. This is not surprising, since as long as a_0/h is sufficiently small, so that the disturbed interface is not too close to the wall, it is the value of the capillary number $Ca_3 = \mu_1 \chi L/\gamma$ and reduced amplitude a_0/L that are most relevant to the evolution of the interface: the channel walls are important only in producing the shear flow.

For example, in figure 5, we present stages in the evolution of an interface for $L/h = 4$, $a_0/h = 0.8$ and $Ca = 1$, corresponding to $a_0/L = 0.2$ and $Ca_3 = 4$, and observe interfacial folding and formation of penetrating fingers. In figure 3(a), we have seen that the analogous motion with $L/h = 2$, $a_0/L = 0.2$, and $Ca_3 = 2$ was stable. For this value of a_0/L, the threshold value of Ca_3 for unstable motion lies between 2 and 4. The

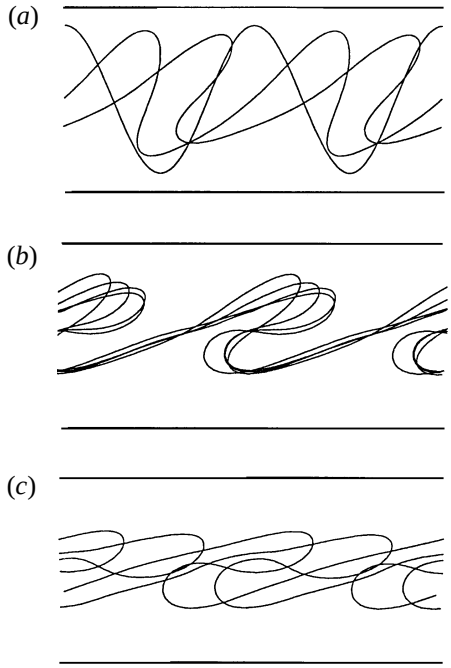

FIGURE 7. Sequences of interfacial profiles for $R = 1$, $\lambda = 5$, $\beta = 1$, $Ca = 2$, $L/h = 2$, and initial amplitude $a_0/h = 0.80$, at (*a*) $t^* = 0$, 1.0, 2.0; (*b*) $t^* = 3.0$, 6.0, 9.1; (*c*) $t^* = 12.1$, 15.0, 19.75.

behaviour of long waves will be discussed further in §3.4 in the context of the long-wave approximation.

3.3. *Effect of the viscosity ratio*

The numerical computations showed that, increasing the viscosity ratio λ while keeping all geometrical parameters and the capillary number Ca fixed, has a profound effect on the character of the motion, and may cause the interface to show permanent deformation of a new kind. We shall illustrate these behaviours with reference to a flow with $R = 1$, $L/h = 2$, $a_0/h = 0.40$, and $Ca = 1$.

In figure 3(*a*), we saw that when $\lambda = 1$, the disturbance decays and the asymptotic shape of the interface at long times is flat. In figure 6(*a*, *b*), we present a sequence of profiles for $\lambda = 5$; note that the upper fluid is more viscous than the lower one. The interface is clearly more reluctant to return to the unperturbed shape than it was for $\lambda = 1$, but not so reluctant as to allow for folding.

Figure 6(*c*, *d*) shows that increasing λ to the value of 10 while holding all other parameters constant causes the interfacial wave to steepen and then evolve slowly developing a sequence of resilient bulges possibly of permanent form. Since the more-viscous fluid is located at the top, the bulges can be interpreted as fingers of the less-viscous fluid penetrating the more-viscous fluid under the action of the shear flow. In this case, it is not clear that folding will occur at long times. The crest of each bulge travels with a phase velocity that is very close to that predicted by the linear theory, $c_P = 0.812\chi h$. Unfortunately, because of the slow evolution, excessive computational cost, on the order of 3 CPU days, places a practical constraint on the computation of the motion at long times.

Stating, however, that increasing λ destabilizes the flow must be interpreted in an appropriate context. The capillary number Ca was defined as $\mu_1 \Delta U/2\gamma$, in terms of the difference in the velocity of the channel walls ΔU, and the viscosity of the lighter fluid.

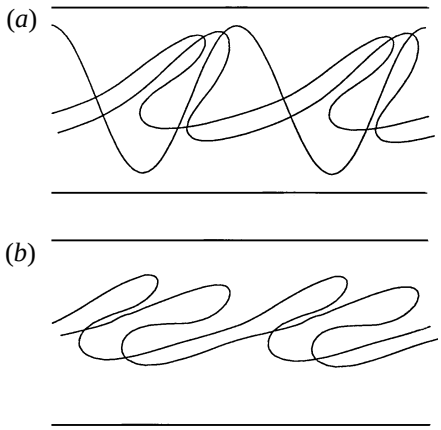

FIGURE 8. Sequences of interfacial profiles for $R = 1$, $\lambda = 10$, $\beta = 1$, $Ca = 2$, $L/h = 2$, and initial amplitude $a_0/h = 0.80$ at (*a*) $t^* = 0$, 2.0, 4.0; (*b*) $t^* = 8.0$, 16.0.

At large values of λ, a more appropriate capillary number is $Ca_4 = \mu_2 \xi_2 h_2/\gamma$, involving the change in the velocity across the upper layer for unidirectional flow, and the viscosity of the upper fluid. The two capillary numbers are related by $Ca_4 = Ca\, 2\lambda R/(\lambda + R)$. For the conditions discussed in the preceding paragraph, $\lambda = 1$, 5, and 10 correspond respectively, to $Ca_4 = 1$, 1.67, 1.82. In this light, it is not surprising that the interface tends to exhibit permanent deformation when λ is raised while Ca is kept constant.

Further numerical results showed that the interface can be destabilized for any value of λ by subjecting it to a perturbation of a sufficiently large amplitude, provided only that Ca is not excessively small. For example, in figures 7 and 8, we present stages in the evolution of a disturbance with $a_0/h = 0.80$, and $Ca = 2$, and $\lambda = 5$ and 10. In both cases, fingers of the less-viscous lower fluid penetrate, and are then enclosed by, the more-viscous upper fluid.

3.4. *Long-wave approximation*

Ooms *et al.* (1985) formulated an approximate theory to describe the evolution of interfacial perturbations whose period is long compared to the channel width. Assuming that the flow is locally unidirectional and the streamwise velocity profile across each layer and at every station is parabolic, and requiring conservation of mass and continuity of shear stress across the interface, they obtained the partial-differential equations

$$\frac{\partial}{\partial x}\left(h_1^3 \frac{\partial p_1^{Mod}}{\partial x}\right) = 6\mu_1(U_1 - u_I)\frac{\partial h_1}{\partial x} + 6\mu_1 h_1 \frac{\partial u_I}{\partial x} + 12\mu_1 v_I, \tag{29a}$$

$$\frac{\partial}{\partial x}\left(h_2^3 \frac{\partial p_2^{Mod}}{\partial x}\right) = 6\mu_2(U_2 - u_I)\frac{\partial h_2}{\partial x} + 6\mu_2 h_2 \frac{\partial u_I}{\partial x} - 12\mu_2 v_I, \tag{29b}$$

where $h_1(x, t)$ and $h_2(x, t)$ are the instantaneous lower and upper layer thickness and $p_1^{Mod}(x, t)$ and $p_2^{Mod}(x, t)$ are the corresponding modified pressures excluding the hydrostatic variation due to gravity. The y velocity component at the interface, v_I, does not participate in the equation of motion but may be computed by requiring conservation of mass expressed by the kinematic boundary condition yielding

$$v_I = \frac{\partial h_1}{\partial t} + u_I \frac{\partial h_1}{\partial x}. \tag{30}$$

Requiring further that the normal stress undergo a jump across the interface, and relating this jump to the magnitude of the surface tension, yields

$$p_2^{Mod} = p_1^{Mod} - \Delta\rho g h_1 + \gamma \frac{\partial^2 h_1}{\partial x^2}, \tag{31}$$

where $\Delta\rho = \rho_1 - \rho_2$. Using (31), we find that the x-component of the velocity at the interface is given by

$$u_I = \frac{1}{\lambda + r}\left[h h_2 \frac{1}{\mu_1}\frac{\partial p_1^{Mod}}{\partial x} + \frac{1}{2}\frac{h_2^2}{\mu_1}\left(\Delta\rho g \frac{\partial h_1}{\partial x} - \gamma \frac{\partial^3 h_1}{\partial x^3}\right) + \lambda U_2 + r U_1\right], \tag{32}$$

where $r(x,t) = h_2(x,t)/h_1(x,t)$ is the local and instantaneous layer thickness ratio.

Combining (29a) and (29b) to eliminate v_I, and then using (31) and (32) to eliminate p_2^{Mod} and u_I, produces the relation

$$\left(\lambda h_1^3 + h_2^3 + 12\frac{\lambda}{\lambda + r} h^2 h_2\right)\frac{1}{\mu_1}\frac{\partial p_1^{Mod}}{\partial x} = \frac{\Delta\rho g}{\mu_1}\left(h_2 + 6\frac{\lambda}{\lambda + r} h\right) h_2^2 \frac{\partial h_1}{\partial x}$$

$$+ 6\lambda(U_1 h_1 + U_2 h_2) - \frac{\gamma}{\mu_1}\left(h_2 + 6\frac{\lambda}{\lambda + r} h\right) h_2^2 \frac{\partial^3 h_1}{\partial x^3} + 12\frac{\lambda}{\lambda + r} h(\lambda U_2 + r U_1) + f(t). \tag{33}$$

The function $f(t)$ arises by specifying the modified pressure drop over one period $\Delta p_1^{Mod} = \Delta p_2^{Mpd} = p_1^{Mod}(x + L, t) - p_1^{Mod}(x, t)$. For the Couette flow considered here, $\Delta p_1^{Mod} = 0$.

Solving (33) for $\partial p_1^{Mod}/\partial x$ and substituting the result into (29a), substituting further the right-hand side of (30) in place of v_I, and the right-hand side of (32) in place of u_I, into (29a), gives a nonlinear evolution equation for the lower layer thickness which we write in the symbolic form

$$\frac{\partial h_1}{\partial t} = F\left(h_1, \frac{\partial h_1}{\partial x}, \frac{\partial^2 h_1}{\partial x^2}, \frac{\partial^3 h_1}{\partial x^3}\right). \tag{34}$$

The right-hand side is a strongly nonlinear function of the arguments of the function F. When the amplitude of the perturbation is small compared to the wavelength, and the surface tension is sufficiently high, (34) reduces to the Kuramoto–Sivashinsky equation (e.g. Charru & Fabre 1994, Section IV).

To generate solutions of (34), we implemented two standard finite-difference methods: an explicit method based on the forward-time central-space discretization, and an implicit method based on the backward-time central-space finite-difference discretization. The spatial step Δx was uniform over a period of the wave, and the time step Δt was adjusted to prevent spurious oscillations. In the implicit method, the nonlinear algebraic system arising from the finite-difference discretization was solved using Newton's method; the Jacobian matrix was computed by numerical differentiation at every iteration. The explicit method performed well for zero or very small values of the surface tension, but numerical instabilities set in at moderate and large values of the surface tension. The implicit method performed well at moderate values of the viscosity ratio even at large values of the surface tension, but the iterations failed to converge at small or large values of the viscosity ratio. Not surprising, both methods yielded spurious oscillations when the interfacial slope became steep. Ooms *et al.* (1985) used an explicit method with upwind differences to overcome the spurious oscillations, but carried out computations only for zero surface tension. With the implicit method, the most demanding computations required less than 15 minutes of CPU time at the facilities described in §2.

The lubrication-flow model is expected to produce reliable results when the characteristic size of the interfacial patterns is large compared to the channel width $2h$. This, of course, requires that the interface can be described in terms of a single-valued function as $y = q(x, t)$, where the magnitude of $\partial q/\partial x$ is small compared to unity. Interfacial folding cannot be captured, but may be indicated by the continuous steepening of the interfacial structures. Our objective is to assess the differences in behaviour predicted by the lubrication-flow model and the unsimplified system of governing equations, when the model is applied on the border of its range of validity.

In figure 9, we compare interfacial profiles computed from the boundary-integral method, shown with the solid lines, to those computed using the lubrication-flow model, shown with the dashed lines. Note that the vertical axis is stretched to show the detailed structure of the interface. In both cases, $Ca = 1$, $\lambda = 1$, and $L/h = 4$; the interfacial wave is only moderately long. The agreement for $a_0/h = 0.10$ shown in figure 9(*a*) is fair: the rate of decay of the interface is significantly overestimated by the lubrication-flow model, and the asymmetry of the developing profile predicted by it is less prominent. The agreement in the rate of decay improves by using the exact expression for the mean curvature instead of the approximation shown in the last term of equation (31) – thereby effectively reducing the importance of the surface tension – but this an *ad hoc* modification that violates the self-consistency of the lubrication approximation. Figure 9(*b*), corresponding to $a_0/h = 0.80$, reveals the inability of the lubrication-flow model to capture the interfacial folding illustrated in figure 5. The crests continue to steepen, but the amplitude of the perturbation continues to decay leading to a different type of behaviour at long times.

Another revealing comparison is presented in figure 9(*c*, *d*), showing corresponding profiles for $Ca = \infty$, that is, zero surface tension, $\lambda = 10$, and $L/h = 4$, obtained using, respectively, the boundary-integral method and the lubrication approximation with the explicit finite-difference method. The boundary-integral computation was stopped when small-scale irregularities developed. Numerical experimentation indicated that these irregularities are not necessarily a numerical artifact but may be a precursor of local penetration. The lubrication-flow computation was stopped when numerical oscillations set in at the crests of the steepening waves, probably requiring upwind differences or a more sophisticated finite-difference method. Significant differences in the shapes of the evolving waves are observed even during the time period when the interface has a smooth shape.

Ooms *et al*. (1985) performed computations for $L/h = 12$, $y_0/h = 0.60$, $a_0/h = 0.20$, and $\lambda = 10^{-5}$, 10^{-4}, 10^{-1}, and suggested the occurrence of steadily travelling steep waves. Their results up to the point where the interfacial wave becomes noticeably steep and artificial oscillations set in were reproduced using our explicit numerical method. Unfortunately, excessive computational cost prevented us from carrying out boundary integral computations for long wavelengths and thus from confirming the motion predicted by the lubrication model.

The comparisons between the predictions of the lubrication model and the results of the numerical simulations discussed in the previous paragraphs suggest that, in the absence of fluid inertia, the physical relevance of steep interfacial waves predicted by the former should be accepted with a certain degree of reservation, especially for waves of moderate wavelength. It is possible that when weak or strong intertial effects are included, the predictions of an approximate theory based on the long-wave approximation will show better agreement with those of a direct numerical simulation, but a critical comparison must await advances at both ends.

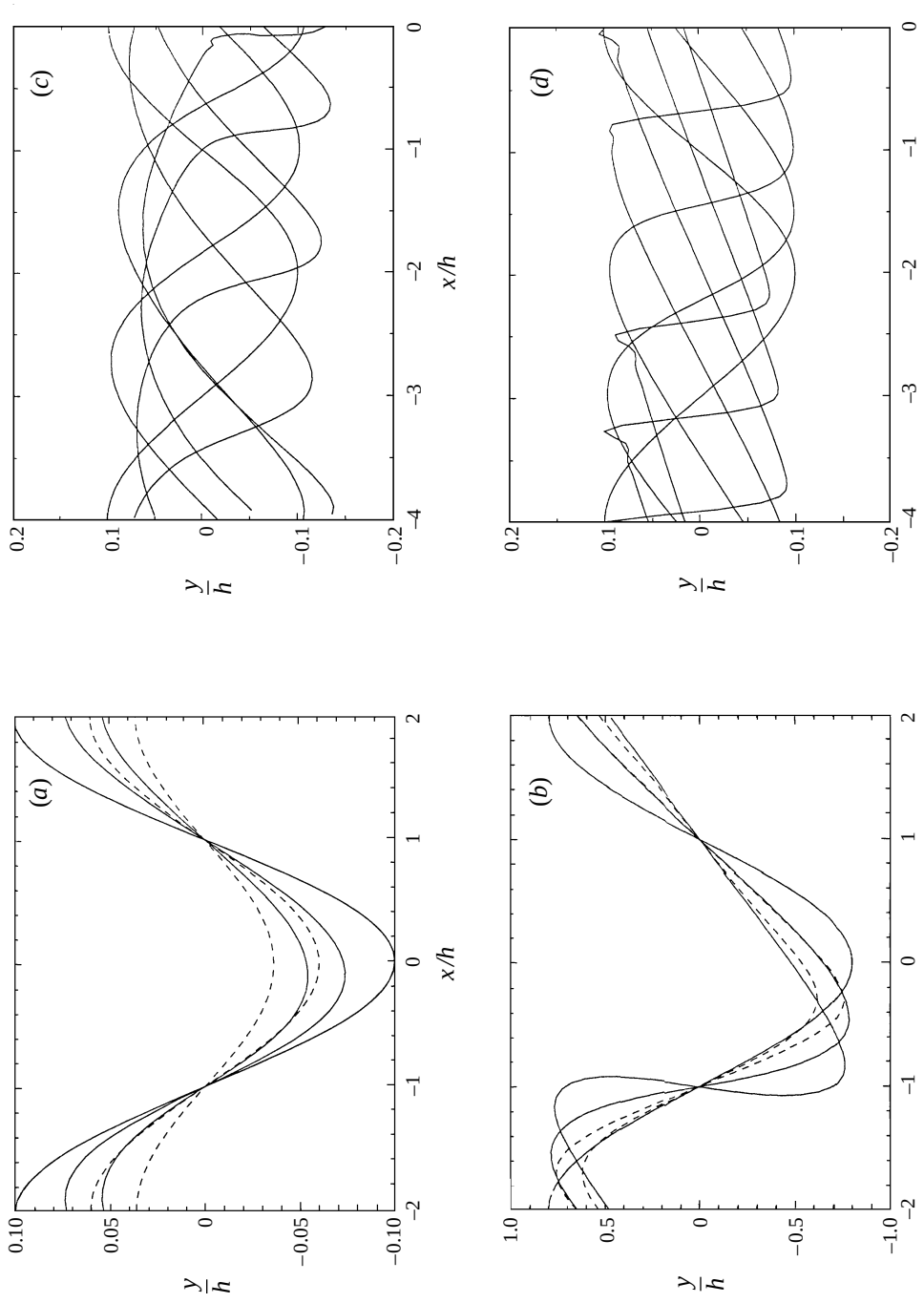

FIGURE 9. Interfacial profiles computed from the boundary-integral method (solid lines), compared to those computed using the lubrication-flow model (dashed lines). (*a*) $R = 1$, $\lambda = 1$, $\beta = 1$, $Ca = 1$, $L/h = 4$, $a_0/h = 0.10$, for $t^* = 0$, 2.0, 4.0. (*b*) Conditions are same as in (*a*) but $a_0/h = 0.80$. (*c*) Results of the boundary-integral method for $R = 1$, $\lambda = 1$, $\beta = 1$, $Ca = \infty$, $L/h = 4$, $a_0/h = 0.10$, for $t^* = 0$, 2.0, 4.0, 6.0, 8.0, 10.0, 11.3; (*d*) corresponding results obtained from the lubrication approximation.

4. Pressure-driven flow

In the second part of the numerical investigation, we consider the stability of the interface in pressure-driven flow depicted in figure 1(*c*). In the problem statement, we retain the assumptions and follow the notation of the preceding section. We stipulate, in particular, that the perturbation does not generate a pressure drop across each periodic cell, and the total pressure drop over a cell ΔP is equal to that of the unperturbed flow. Physically, the motion is generated by a pump that operates at a constant pressure head but variable flow rate.

The motion of the interface depends on the viscosities of the two fluids μ_1 and μ_2, the interfacial tension γ, the unperturbed layer thicknesses h_1 and h_2, the negative of the effective pressure gradient $G = -\Delta P/L$, and the wavelength and amplitude of the interfacial wave L and a_0. To study the behaviour of the flow in a channel of specified dimensions while varying the properties of the fluids, we reduce all lengths by the channel semi-width h, time by μ/Gh, stresses by Gh, and introduce the capillary number $Ca = Gh^2/\gamma$. The four parameters of the flow are Ca, $\lambda = \mu_2/\mu_1$, $R = h_2/h_1$, L/h, and a_0/h.

4.1. *Linear theory*

As in the case of Couette flow, linear theory predicts that, so long as a_0/h and a_0/L are sufficiently small, a sinusoidal perturbation decays for any finite value of the capillary number. The evolution of the interfacial wave is described by equations (26) and (27). Expressions relating c_P and σ_I to the various parameters of the flow arise from those for Couette flow discussed in the previous section by substituting the unperturbed velocity and velocity gradients at the interface. A FORTRAN program that produces c_P and σ_I may be obtained by the author on request.

4.2. *Results of the numerical investigation*

The primary goal of our numerical investigation is to resolve whether the parabolicity of the velocity profile of the unperturbed flow due to the mean pressure gradient has a fundamental effect on the character of the motion. In this section, we focus our attention on the flow of two layers of equal thickness, $R = 1$, and reserve comments for the effect of R for the concluding §5.

First, we study the effect of the reduced amplitude of the perturbation a_0/h on the flow of two layers of equal viscosity, $\lambda = 1$, for reduced wavelength $L/h = 2$. Since the unperturbed interface is located at the channel centreline, the local shear rate of the parabolic flow is equal to zero. Thus, the present set of conditions complements those for shear-driven flow considered in the preceding section. To avoid repetition, in the following discussion we point out the salient new features and main differences from the case of shear-driven flow, and consider the similarities to be implicit. The motion of the interface is described in a frame of reference that translates with the velocity of the unperturbed interface.

The numerical results for small-amplitude perturbations are in excellent agreement with the predictions of the linear theory. In figure 10 we plot, on a log-linear scale, the ratio $a(t)/a_0$ for $Ca = 0.05$ and $a_0/h = 0.20$, and observe a nearly exponential decay. The predictions of the linear theory are represented by the straight line whose slope is equal to -0.01127. For the small amplitude $a_0/h = 0.001$, the rate of decay extracted from the numerical results agrees with the linear analysis to the third significant figure.

As the initial amplitude of the perturbation is raised, the disagreement between the linear theory and the numerical computations becomes more pronounced, and the evolution of the interface becomes increasingly more involved. In figure 11(*a*), we

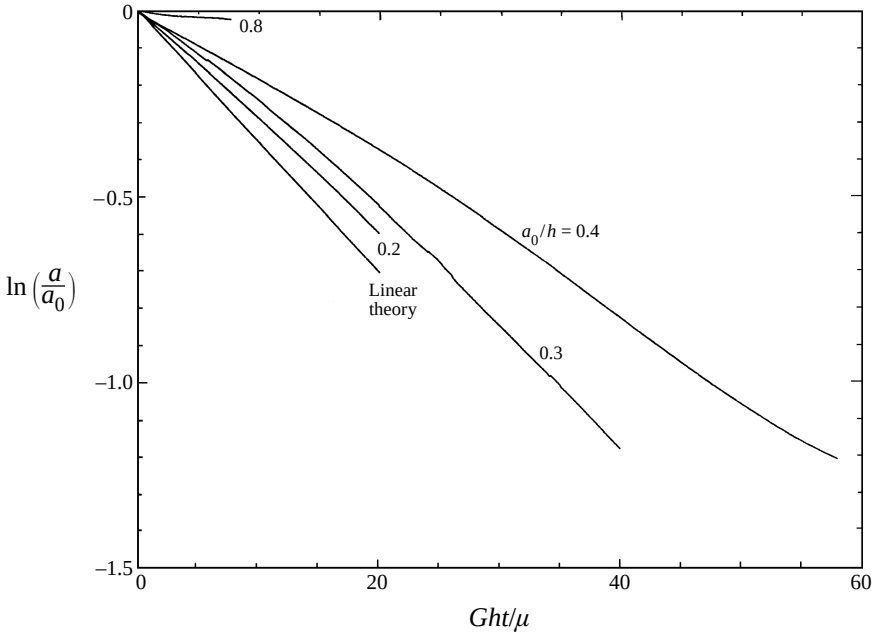

FIGURE 10. Evolution of the maximum height of the interface of two layers of equal thickness in Poiseuille flow, $R = 1$, for fluids of equal viscosity, $\lambda = 1$, equal density, $\beta = 1$, $Ca = 0.05$, reduced wavelength $L/h = 2$, and for perturbations of different initial amplitudes. The straight line represents the predictions of the linear theory.

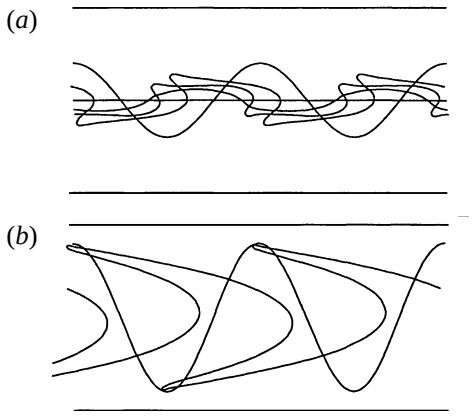

FIGURE 11. Sequences of interfacial profiles for $R = 1$, $\lambda = 1$, $\beta = 1$, $Ca = 0.05$, $L/h = 2$, and initial amplitude (*a*) $a_0/h = 0.40$ at $t^* = Ght/\mu = 0$, 20.0, 40.0, 58.0; (*b*) $a_0/h = 0.80$ at $t^* = 0$, 7.0.

present a sequence of interfacial profiles for a disturbance with initial amplitude $a_0/h = 0.40$. At early times, the interface tends to attain a piecewise parabolic shape corresponding to the velocity profile of the unperturbed flow, while the amplitude of the disturbance is being reduced due to the surface tension. The competition between the advective motion of the incident flow and the restraining action of surface tension leads to the formation of an alternating row of half-arrow shapes. Eventually, the surface tension dominates, and the interface returns to the flat shape. The folding and unfolding of the interface are familiar from the case of Couette flow discussed in the preceding section, but the transient shapes in Poiseuille flow are much more striking.

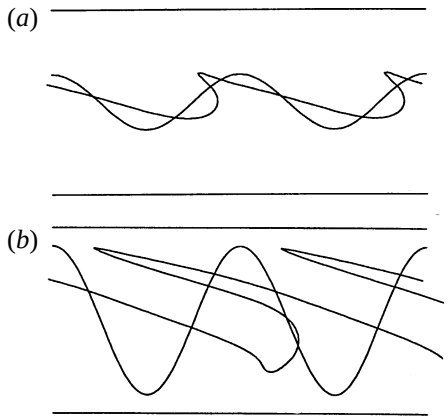

FIGURE 12. Sequences of interfacial profiles for $R = 1$, $\lambda = 10$, $\beta = 1$, $Ca = 0.05$, $L/h = 2$, and initial amplitude (*a*) $a_0/h = 0.30$ at $t^* = Ght/\mu = 0$, 23.35; (*b*) $a_0/h = 0.80$ at $t^* = 0$, 25.0.

The reflection of the half-arrow shapes shown in figure 11(*a*) across the centreline yields closed full-arrow shapes with high curvature at the front and a dimple at the back. It is interesting to note that such shapes are obtained during the motion of drops through a channel when the capillary number is sufficiently large, for both pressure-driven and gravity-driven flow. This and previous observations suggest that the most corrugated portions of the interface develop in a manner that is familiar from studies of the motion of viscous drops.

Raising the initial amplitude of the perturbation to the value $a_0/h = 0.80$ leads to permanent deformation, as shown in figure 11(*b*). In this case, the surface tension is not strong enough to prevent filamentation. The critical amplitude of the perturbation above which the interface does not return to the flat shape can be estimated by arguments that are similar to those presented in the preceding section for Couette flow, but there is some subjectivity due to an adjustable parameter involved in the derivation.

Similar behaviours are observed for higher and lower values of the capillary number. For each reduced wavelength L/h, there is a critical amplitude of the disturbance that is a monotonically increasing function of the capillary number, above which the interface exhibits permanent deformation. When the capillary number is infinite, that is, in the absence of surface tension, the interface is simply convected as a material line by the parabolic flow.

The effect of the viscosity ratio λ is similar to that discussed in the preceding section for Couette flow. Increasing or decreasing λ from the value of unity, while holding all other parameters constant, promotes the growth of the interfacial waves. For example, in figure 12, we show typical stages in the evolution of the interface for $Ca = 0.05$, $\lambda = 10$, $L/h = 2$, and $a_0/h = 0.30$ and 0.80. In the first case, the interface develops a periodic sequence of spikes of the less-viscous lower fluid projecting into the more-viscous upper fluid. The computation was stopped when the curvature at the crest has become so small that an extremely small time step was necessary in order to prevent numerical instabilities. There is no evidence that the perturbation will decay at long times. We note that, in the corresponding motion for $\lambda = 1$, the interface returns to the flat shape at long times, and this underscores once more the destabilizing effect of the viscosity ratio. The evolution for $a_0/h = 0.80$ depicted in figure 12(*b*) is similar to that for $a_0/h = 0.30$, but the spikes are longer and more slender, and the lower part of the interface tends to conform with the piecewise parabolic profile of the unperturbed flow.

As in the case of Couette flow, it can be argued that a parametric investigation where Ca is fixed and λ is varied is not fully revealing, and that the capillary number should be redefined with respect to the unperturbed velocity difference across the more-viscous fluid. This argument would give a partial reason why the waves grow as λ is raised.

5. Discussion

We have presented numerical results for layers of equal thicknesses corresponding to $R = 1$. Computations with layers of unequal thicknesses revealed similar behaviours with only qualitative differences. In the case of pressure-driven flow, varying the relative layer thickness amounts to altering the rate of change of the shear rate with respect to transverse distance across the channel, evaluated at the position of the unperturbed interface. Linear analysis and the numerical computations discussed in previous sections indicate that the parabolicity of the unperturbed profile affects the behaviour of the interface in only a qualitative manner.

For example, in figure 13(a, b) we present stages in the evolution of a thin layer attached to a wall in pressure-driven flow, for $Ca = 0.05$, $R = 9$, $L/h = 2$, $a_0/h = 0.10$, and $\lambda = 5$ and 10. Note that the wall layer is less viscous than the overlying fluid. The interface continues to evolve beyond the final stage shown in figure 13(a), but the computation was too expensive to continue. The computation for $\lambda = 10$ was stopped when regions of high curvature developed at the bases of the forming bulges, possibly indicating local penetration.

The final shape shown in figure 13(b), which however continues to evolve, is similar to the steady shape of a wavy interface in axisymmetric lubricated core flow (Bai *et al.* 1996); the earlier transient shapes are similar to those computed by Yiu & Chen (1996) and Coward *et al.* (1997) for two-dimensional layered flow at low and moderate Reynolds numbers. That the interface does not seem to reach a steady shape may be attributed to the absence of fluid inertia: the observations of Barthelet *et al.* (1995) suggest that inertial effects restrain the continuous deformation and lead to saturation. Furthermore, it is possible that the establishment of steadily travelling waves requires larger values of the viscosity ratio, although, according to weakly nonlinear theory, it is more likely that the bifurcation to a travelling wave be supercritical when the viscosity ratio is moderate rather than extreme. In the oil–water core–annular flow occurring in engineering practice, where steady shapes have been oberved, the viscosity ratio may be on the order of 500.

Numerical computations for large viscosity ratios and small or zero surface tension revealed the spontaneous development of regions of high interfacial curvature at the tips of the interfacial spikes. An example is shown in figure 12(b). Regrettably, the large computational cost required for the computation of the Green's function prevented us from studying the analytic structure of the interfacial shapes near the regions of high curvature, and the computations were stopped when the local curvature became so large that an excessively small time step was required. There is a resurgence of interest in corner and cusp formation along two-dimensional interfaces in Stokes flow, and recent work has shown that such singularities may occur under a broad range of conditions (e.g. Pozrikidis 1997b). Richardson (1997) found that transient cusps may occur even when the surface tension is non-zero. The flows considered in this paper are not particularly well suited to studies of singularity formation, although they may serve as prototypical models for laboratory investigations.

The results of the present numerical study contribute to our understanding of mixing due to mechanical agitation, in the sense that they illustrate the local behaviour of a

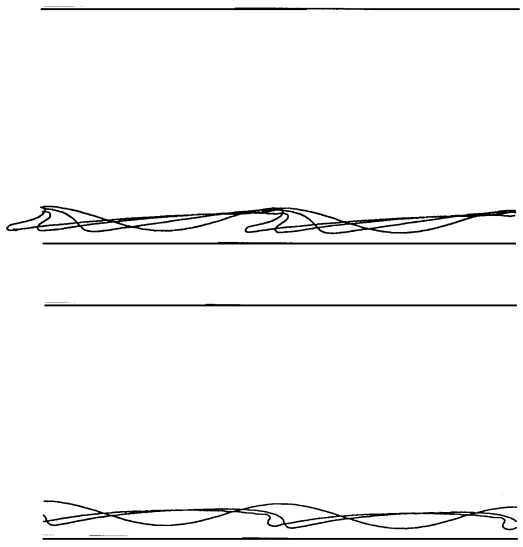

FIGURE 13. Sequences of interfacial profiles for $R = 9$, $\beta = 1$, $Ca = 0.05$, $L/h = 2$, $a_0/h = 0.10$; (*a*) $\lambda = 5$, $t^* = Ght/\mu = 0$, 10, 20, 26; (*b*) $\lambda = 10$, $t^* = 0$, 28.0, 36.5.

non-flat interface under conditions of nearly unidirectional flow. Partial information on the behaviour of interfaces in a purely straining ambient flow can be inferred from analytical and numerical studies of bubble and drop deformation in linear flows. Tjahjadi & Ottino (1991) studied the stretching and disintegration of a drop in two-dimensional journal-bearing flow under conditions of chaotic advection, and identified the significance of the local structure of the flow and of the physical properties of the fluids. Analogous studies with large blobs or layers of stratified fluid subjected to carefully designed flows will illuminate the micro-physics of heterogeneous mixing in viscous flows.

I am indebted to Professors Y. Y. Renardy and M. Renardy for making me aware of their recent numerical simulations. Madhu Gopalakrishnan assisted me in the formulation of the linear stability problem. This research was supported by the National Science Foundation and the SUN Microsystems Corporation. Acknowledgement is made to the Donors of the Petroleum Research Fund, administered by the American Chemical Society, for partial support.

REFERENCES

ANTURKAR, N. R., PAPANASTASIOU, T. C. & WILKES, J. O. 1990 Linear stability analysis of multilayer plane Poiseuille flow. *Phys. Fluids* A **2**, 530–541.

BAI, R., KELKAR, K. & JOSEPH, D. D. 1996 Direct simulation of interfacial waves in a high-viscosity-ratio and axisymmetric core-annular flow. *J. Fluid Mech.* **327**, 1–34.

BARTHELET, P., CHARRU, F. & FABRE, J. 1995 Experimental study of interfacial long waves in a two-layer shear flow. *J. Fluid Mech.* **303**, 23–53.

CHARRU, F. & FABRE, J. 1994 Long waves at the interface between two viscous fluids. *Phys. Fluids* **6**, 1223–1235.

CHEN, K. 1990 Wave formation in the gravity-driven low-Reynolds-number flow of two liquid films down an inclined plane. *Phys. Fluids* A **5**, 3038–3048.

COWARD, A. V., RENARDY, Y. Y., RENARDY, M. & RICHARDS, J. R. 1997 Temporal evolution of periodic disturbances in two-layer Couette flow. *J. Comput. Phys.* **132**, 346–361.

Han, C. D. 1981 *Multiphase Flow in Polymer Processing*. Academic.

Hesla, T. I., Pranckh, F. R. & Preziosi, L. 1986 Squire's theorem for two stratified fluids. *Phys. Fluids* **29**, 2808–2811.

Hinch, E. J. 1984 A note of the mechanism of the instability at the interface between two shearing fluids. *J. Fluid Mech.* **14**, 463–465.

Hooper, A. P. 1985 Long-wave instability at the interface between two viscous fluids. *Phys. Fluids* **28**, 1613–1618.

Hooper, A. P. 1989 The stability of two superposed viscous fluids in a channel. *Phys. Fluids* **1**, 1133–1142.

Hooper, A. P. & Grimshaw, R. 1985 Nonlinear instability at the interface between two viscous fluids. *Phys. Fluids* **28**, 37–45.

Jana, S., Metcalfe, G. & Ottino, J. M. 1994 Experimental and computational studies of mixing in complex Stokes flows: the vortex mixing flow and multicellular cavity flows. *J. Fluid Mech.* **269**, 199–246.

Joseph, D. D. & Renardy, Y. Y. 1992 *Fundamentals of Two-Fluid Dynamics*. Springer.

Kao, M. E. & Park, C. 1972 Experimental investigation of the stability of channel flow. *J. Fluid Mech.* **52**, 401–423.

Kliakhandler, I. L. & Sivashinsky, G. I. 1997 Viscous damping and instabilities in stratified liquid film flowing down a slightly inclined plane. *Phys. Fluids* **9**, 23–30.

Li, C.-H. 1969 Instability of three-layer viscous stratified flow. *Phys. Fluids* **12**, 2473–2481.

Loewenherz, D. S. & Lawrence, C. J. 1989 The effect of viscosity stratification on the stability of a free surface flow at low Reynolds number. *Phys. Fluids* A **1**, 1686–1693.

Ooms, G., Segal, A., Cheung, S. Y. & Oliemans, R. V. A. 1985 Propagation of long waves of finite amplitude at the interface of two viscous fluids. *Intl. J. Multiphase Flow* **11**, 481–502.

Ottino, J. M. 1989 *The Kinematics of Mixing: Stretching, Chaos, and Transport*. Cambridge University Press.

Pozrikidis, C. 1992 *Boundary Integral and Singularity Methods for Linearized Viscous Flow*. Cambridge University Press.

Pozrikidis, C. 1997*a* *Introduction to Theoretical and Computational Fluid Dynamics*. Oxford University Press.

Pozrikidis, C. 1997*b* Numerical studies of singularity formation at fluid interfaces in two-dimensional Stokes flow. *J. Fluid Mech.* **331**, 145–167.

Renardy, M. & Renardy, Y. 1993 Derivation of amplitude equations and analysis of sideband instabilities in two-layer flows. *Phys. Fluids* A **5**, 2738–2762.

Renardy, Y. 1985 Instability at the interface between two shearing fluids in a channel. *Phys. Fluids* **28**, 3441–3443.

Richardson, S. 1997 Two-dimensional Stokes flows with time-dependent free boundaries driven by surface tension. *Eur. J. Appl. Maths* **8**, 311–329.

Shlang, T., Sivashinski, G. I., Babchin, A. J. & Frenuel, A. L. 1985 Irregular wavy flow due to viscous stratification. *J. Phys. Paris* **46**, 863–866.

Su, Y. Y. & Khomami, B. 1992 Numerical solution of eigenvalue problems using spectral techniques. *J. Comput. Phys.* **100**, 297–305.

Tilley, B. S., Davis, S. H. & Bankoff, S. G. 1994*a* Linear stability theory of two-layer fluid flow in an inclined channel. *Phys. Fluids* **6**, 3906–3922.

Tilley, B. S., Davis, S. H. & Bankoff, S. G. 1994*b* Nonlinear long-wave stability of superposed fluids in an inclined channel. *J. Fluid Mech.* **277**, 55–83.

Tjahjadi, M. & Ottino, J. M. 1991 Stretching and breakup of droplets in chaotic flows. *J. Fluid Mech.* **232**, 191–219.

Weinstein, S. J. & Kurz, M. R. 1991 Long-wavelength instabilities in three-layer flow down in incline. *Phys. Fluids* **3**, 2680–2687.

Yiantsios, S. & Higgins, B. G. 1988 Linear stability of plane Poiseuille flow of two superposed fluids. *Phys. Fluids* **31**, 3225–3238.

Yih, C. S. 1967 Instability due to viscosity stratification. *J. Fluid Mech.* **27**, 337–352.

Yiu, R. R. & Chen, K. P. 1996 Numerical experiments on disturbed two-layer flows in a channel. In *Advances in Multi-Fluid Flows* (ed. Y. Renardy, A. V. Coward, D. Papageorgiou & S. M. Sun), pp. 368–382, SIAM.

Zaleski, S., Li, J., Scardovelli, R. & Zanetti, G. 1996 Direct simulation of multiphase flows with density variations. *Colloque IUTAM*, *Marseille*. Kluwer.

Zhou, H. & Pozrikidis, C. 1993 The flow of suspensions in channels: single files of drops. *Phys. Fluids* A **5**, 311–324.